Fuel 184 (2016) 36–41

Contents lists available at ScienceDirect

Fuel

journal homepage: www.elsevier.com/locate/fuel

Full Length Article

Novel reductive extraction process to convert the bio-oil aqueous acid fraction into fuels with the recovery of iron from wastes

Fernanda G. Mendonça [a], Jamerson P.M. Gomes [a], Juliana C. Tristão [b], José D. Ardisson [c], Ricardo R. Soares [d], Rochel M. Lago [a,*]

[a] Departamento de Química, Instituto de Ciências Exatas, Universidade Federal de Minas Gerais, Belo Horizonte, MG, Brazil
[b] Universidade Federal de Viçosa – Campus Florestal, Florestal, MG, Brazil
[c] Centro de Desenvolvimento da Tecnologia Nuclear, Belo Horizonte, MG, Brazil
[d] Departamento de Engenharia Química, Universidade Federal de Uberlândia, Uberlândia, MG, Brazil

HIGHLIGHTS

- Bio-oil aqueous acid fraction efficiently extracts iron of the red mud waste.
- $Fe_{extracted}$/aqueous fraction is converted into Fe/C composites valuable for the steel industry.
- The organics are decomposed to a potential fuel gas mixture consisting of H_2/hydrocarbon.

ARTICLE INFO

Article history:
Received 4 May 2016
Received in revised form 15 June 2016
Accepted 20 June 2016
Available online 7 July 2016

Keywords:
Bio-oil aqueous acid fraction
Metal extraction
Red mud

ABSTRACT

In this work, bio-oil waste AAF (aqueous acid fraction) was used to recover iron from red mud (RM) waste by a reductive extraction process. In this process, extraction of iron from RM with AAF is followed by thermal treatment of AAF-$Fe_{extracted}$ mixture, leading to the reduction of the $Fe_{extracted}$ with the production of Fe/C composites, a valuable feedstock for the steel industry, and a gas fuel fraction. Analyses by IR, UV–vis, ESI-MS, CHN, potentiometric titration, TG, TG-MS, TOC and ^{1}H NMR showed AAF can efficiently extract Fe^{3+} present in RM waste. After extraction, the mixture AAF-$Fe_{extracted}$ was treated at 400, 600 and 800 °C to decompose mainly into two fractions: solid (30–40 wt%) and gas (60–70 wt%). Mössbauer and XRD analyses of the solid fraction showed the presence of reduced iron phases, *e.g.* Fe^{2+}, Fe^0 and iron carbide, with 76% of carbon. TG-MS analyses of gas fraction showed the production of H_2 (58 mol%), C_1–C_4 (19 mol%) and CO_x (23 mol%), with potential application as a fuel.

1. Introduction

Bio-oil is produced by flash pyrolysis of lignocellulosic biomass at relatively high temperatures, *e.g.* 500–650 °C, in the absence of oxygen. The three fractions produced in this process are bio-char, bio-oil and bio-gas, with typical yields of ca. 15–25, 60–75 and 5–15%, respectively. In this process, significant amounts of water are also formed, which is dragged with bio-oil producing two distinct immiscible liquid phases: bio-oil (approximately 80%) and the aqueous acid fraction (ca. 20%) [1–4].

Aqueous acid fraction (AAF) is a dark liquid comprising approximately 75–85% of water and 15–25% of organic compounds [5–7] as small carboxylic acids (C_1–C_3), and other oxygenated compounds such as aldehydes and ketones [8–10]. This aqueous fraction is considered a waste and a drawback in pyrolytic process [6]. Different studies have investigated several pyrolysis conditions in order to minimize AAF's production [6,7,11] and few works in literature have studied its possible applications. Some of the applications investigated involve the mixture of AAF with bio-oils to be used as liquid fuel for gas turbines [8], AAF as raw material for the production of lipids by yeast [12] and steam reform of AAF to produce hydrogen [13–15].

In this work, aqueous acid fraction (AAF) from bio-oil was tested in a process of iron reductive extraction from a Fe rich waste, *i.e.* red mud (RM). In this process, named "2W2P" (two wastes two products), AAF is used to solubilize iron from RM waste. In a posterior step of thermal treatment, the organic matter present in acid fraction carbonizes and reduces the extracted iron to form a Fe/C composite and a gas fraction with potential application as fuel (Eqs. (1) and (2); Fig. 1).

* Corresponding author.
E-mail address: rochel@ufmg.br (R.M. Lago).

http://dx.doi.org/10.1016/j.fuel.2016.06.099
0016-2361/

Fig. 1. Schematic representation of the 2W2P (two wastes two products) process.

$$Fe^{3+}_{rich\ waste}(RM) + AAF \rightarrow Fe^{3+}_{extracted}/AAF \quad (1)$$

$$Fe^{3+}_{extracted}/AAF \rightarrow Fe/carbon + fuels_{(gas)} \quad (2)$$

Red mud (RM) waste is produced in Bayer process of bauxite conversion to aluminum at 90 million ton/year worldwide [16]. Several applications have been studied for this waste, such as production of carbon nanotubes and nanofibers composites [17,18], indirect storage of natural gas [19], reduction of Cr(VI) [20], and also bio-oil upgrade [21,22]. As RM contains high concentrations of Fe, *e.g.* 40 wt%, the idea of iron recovery is very attractive. However, due to the strong interaction and dispersion of the iron oxide with impurities (Al_2O_3 and SiO_2 particles), physical separation is not possible. More complex processes have been used to recover iron and titanium from RM, such as smelting reduction of RM and direct reduction roasting followed by magnetic separation [23,24]. Attempts to convert the RM into a coagulant by Fe^{3+} dissolution in concentrated hydrochloric acid have also been suggested [25,26]. However, these processes are limited by the high costs.

Hereon, a reductive extraction process is described, where Fe^{3+} from RM is extracted and complexed with organic molecules and then thermally treated, leading to the formation of two products: reduced Fe dispersed in a carbon matrix (with potential use in steel industry) as well as hydrogen and small hydrocarbons with potential application as fuel.

2. Materials and methods

2.1. Characterizations

Potentiometric titrations of AAF were carried out with 0.5 mL of sample in 35 mL of KOH 0.091 mol L^{-1}. HCl 0.097 mol L^{-1} was used as titrant and the potential during titration was measured in a PHS-3C Bench pHmeter. Total organic carbon analysis was carried out in a Shimadzu TOC-V CPH. Thermogravimetric analyses (TG/DTA) were carried out in a Shimadzu TGA-60 (10 °C min^{-1} under air or nitrogen flow). UV–vis spectra were obtained in a Shimadzu UV 2550 equipment. ^1H NMR spectra were recorded at room temperature in a Bruker DPX-200 Avance spectrometer, using d-chloroform as solvent. Infrared spectra (IR) were recorded in a Bruker ALPHA equipment, in the wavelengths between 4000 and 400 cm^{-1}, with 64 scans per sample. Elemental analyses were performed in a Perkin Elmer 2400 equipment. Mass spectrometry with electrospray ionization (ESI-MS) was performed in a Thermo Electron spectrometer, model LCQ Fleet, in the positive mode. Powder X-ray diffraction (XRD) data were obtained in a Rigaku equipment model Geigerflex using Cu Kα radiation, scanning from 10 to 80° (2θ) at a scan rate of 4° min^{-1}. Atomic absorption analyses were performed in a Hitachi-Z8200 equipment. Transmission Mössbauer spectroscopic experiments were carried out in a CMTE spectrometer model MA250 with a ^{57}Co/Rh source at room temperature using α-Fe as reference. Raman spectra were recorded in a Bruker Senterra equipment, using 532 nm laser with 5 mW. Thermogravimetric-mass spectrometry (TG-MS) analyses were performed in a NETZSCH equipment model STA 449 F3, coupled to a mass spectrometer NETZSCH Aëolos model QMS 403C, using argon as carrier gas.

2.2. Acid extraction experiments

Acid extraction experiments were carried out in sealed flasks, with a mixture comprised of 5 mL of aqueous acid fraction and 500 mg of red mud. The flasks were kept at 100 °C in an oil bath for 8, 24, 48 and 72 h. Other reactions were carried out with 5 mL of aqueous acid fraction with different amounts of red mud (50–500 mg) at 100 °C for 48 h. After reactions, the mixtures of aqueous acid fraction and red mud were centrifuged for an hour to separate the silica/alumina byproduct, and the supernatant was removed. In order to determine the content of iron extracted from red mud, the supernatant was mineralized with concentrated nitric acid at 80 °C and analyzed by atomic absorption, as previously described.

2.3. Thermal treatment of $Fe^{3+}_{extracted}$/aqueous acid fraction (AAF)

The product obtained after 48 h of reaction of aqueous acid fraction and red mud (AAF/Fe) was thermally treated at different temperatures, *e.g.* 400, 600 and 800 °C. The treatments were carried out with 1 g of AAF/Fe under N_2 atmosphere (50 mL min^{-1}), in a quartz tube into a horizontal furnace (BLUE M. Lindberg) at a heating rate of 10 °C min^{-1}, keeping the final temperature for 1 h. These treatments lead to the formation of a black magnetic solid, a liquid and a gas fraction.

3. Results and discussion

The aqueous acid fraction (AAF) used in this work is a slightly viscous liquid containing high concentration of acidic organic molecules. Characterization of AAF by potentiometric titrations showed negative pH with acid concentration of ca. 3 mol L^{-1}. Total Organic Carbon analysis indicated carbon concentration of 154 g_{Carbon} L^{-1} (ca. 15 wt%). TG/DTA analysis of aqueous acid fraction presented an endothermic event related to water loss (approximately 70 wt%), followed by an exothermic weight loss of 30% related to degradation/oxidation of organics in AAF (Fig. S1). UV–vis analysis (Fig. S2) indicated the presence of bands centered at 218 and 264 nm related mainly to small concentrations of benzene and naphthalene derivatives [27]. ^1H NMR spectrum of AAF (Fig. 2), which is soluble in d-chloroform, exhibited peaks in the range of 1.0–2.5 ppm related to H bonded to aliphatic carbon atoms (γ-CH_3, β-CH_3, CH_2 and γ-CH or further from an aromatic ring) [28]. The peaks between 3.5 and 5.0 ppm are related to H bonded to C-O, and the small peaks between 6.5 and 7.0 ppm indicate the presence of H bonded to aromatic species [29,30].

IR spectra obtained for the dried AAF_{powder} (powder obtained after evaporation of water, Fig. S3) showed the presence of bands related to oxygenated groups, *e.g.* O-H stretching around 3500 cm^{-1} combined with the bands in 1780 cm^{-1} (C═O) and 1290 cm^{-1} (C—O), likely related to phenolic and carboxylic groups. The bands around 1650 and 1450 cm^{-1} can be attributed to C═C stretching of aromatic structures.

Elemental analysis of the dried AAF_{powder} showed ca. 49% C, 6% H and likely 45% oxygen, suggesting the presence of highly oxygenated molecules. ESI-MS analysis indicates the presence of three main groups of molecules containing up to C_{10}, C_{10}–C_{30} and some signals related to molecules higher than C_{30} (Fig. S4).

Fe rich waste used in this work, red mud (RM), showed by XRD the presence of hematite (α-Fe_2O_3, PDF 1-1053), silica (SiO_2, PDF 1-424), alumina (Al_2O_3, PDF 10-414), calcium oxide (CaO, PDF

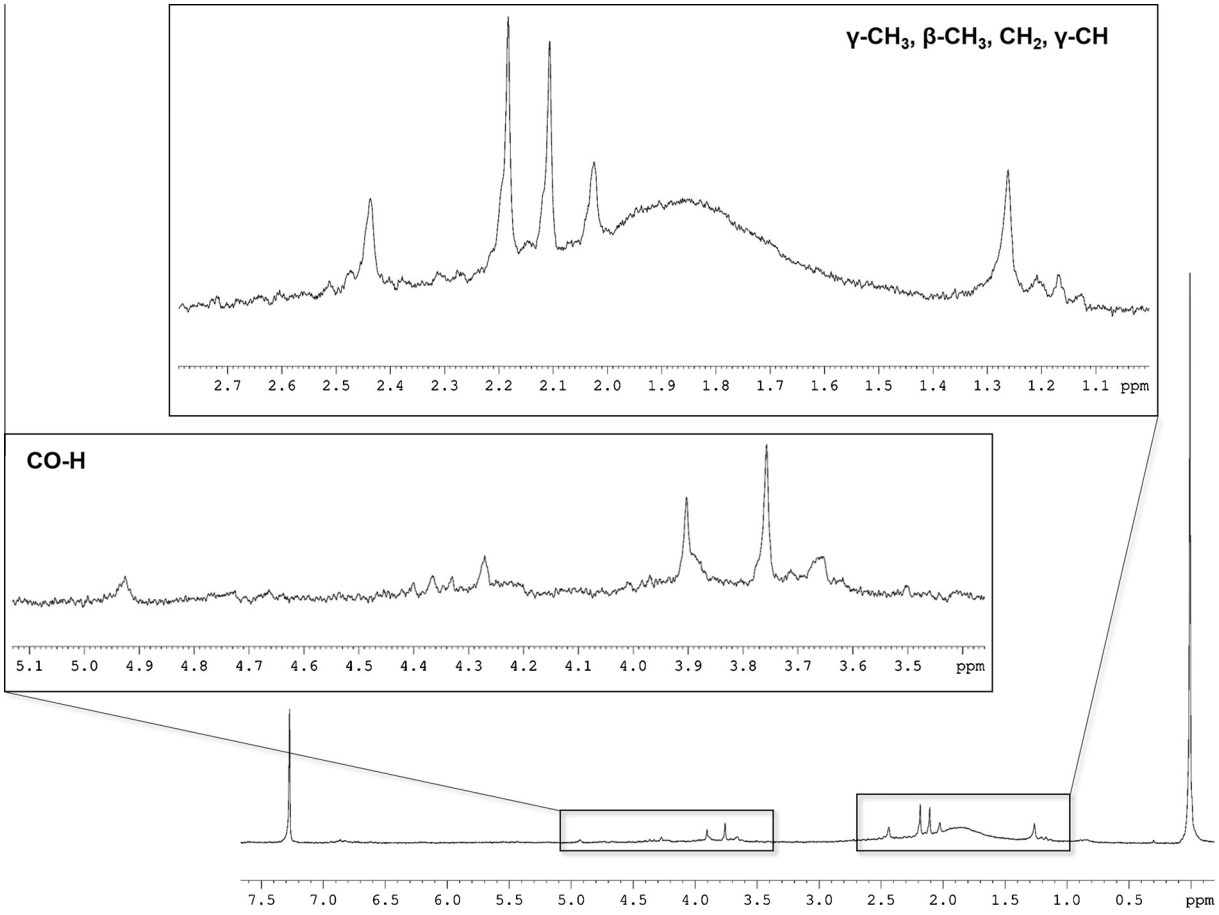

Fig. 2. ^{1}H NMR obtained in $CDCl_3$ and for aqueous acid fraction.

337-1497) and titania (TiO_2, PDF 10-63) (Fig. S5). Atomic absorption analyses showed Fe_2O_3 content of 47 wt%. Mössbauer spectroscopy confirmed the presence of hematite, represented by a sextet with characteristic hyperfine parameters of α-Fe_2O_3 phase. It was also observed a superparamagnetic Fe(III) phase (with 52% spectral area), represented by a doublet in the central region of spectrum (Fig. S6). This superparamagnetic phase is related to a highly dispersed iron oxide, nanometric/amorphous phase present in RM waste.

Iron extractions from RM waste using AAF were carried out at 100 °C with extraction times of 8, 24, 48 and 72 h. Results showed 90% efficiency after 48 h (Fig. 3). Small amounts of Al extracted were also observed, probably originated by the dissolution of aluminum oxides present in RM. No significant extraction of Ti was observed in preliminary atomic absorption analyses.

The effect of the ratio red mud (wt)/AAF (vol) on iron extraction (Fig. S7) was also investigated. It was observed that up to 100 mg_{RM}/mL_{AAF} the extraction of iron from red mud was almost complete. As the ratio increased to 150 mg_{RM}/mL_{AAF}, Fe extraction strongly decreased. Simple titrations and pH measurements sug-

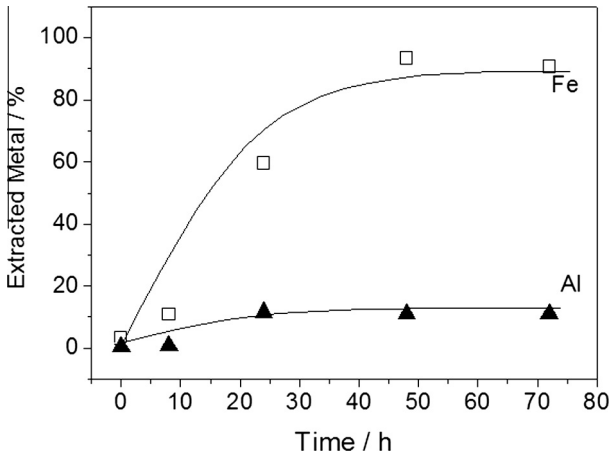

Fig. 3. Extraction of Fe and Al (%) from RM after reactions with AFF at 100 °C.

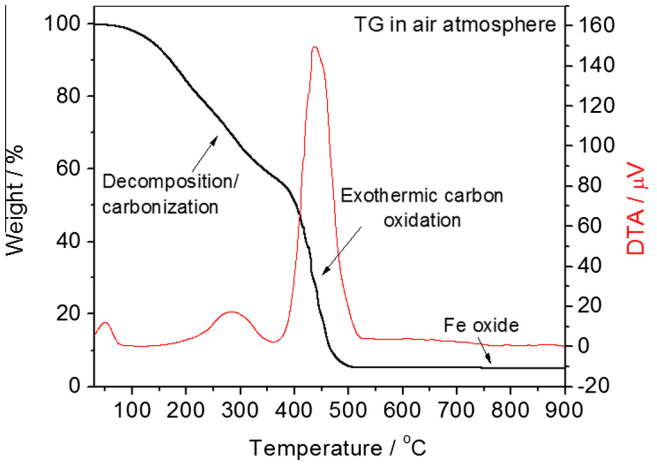

Fig. 4. TGA and DTA curves obtained under air atmosphere for the black solid AAF/Fe_{powder}.

gested that this limitation is related to the complete consumption of acidity of aqueous phase.

Although extraction mechanism is not clear, one can envisage that it takes place by the reaction of surface Fe oxides with H^+ (Eq. (3)) and also by the complexation with organic oxygenates present, *e.g.* carboxylic acids (Eq. (4)).

$$Fe_2O_3 + H^+ \rightarrow Fe^{3+}_{aq} + H_2O \quad (3)$$

$$Fe^{3+}_{surf} + HOOC - R_{aq} \rightarrow [Fe^{3+}(^-OOCR)_n]_{aq} + nH^+_{aq} \quad (4)$$

The obtained $Fe^{3+}_{extracted}$/AAF mixture was dried at 80 °C overnight in order to obtain a black solid, named as AAF/Fe_{powder}. IR spectrum obtained for the solid AAF/Fe_{powder} (Fig. S8) was similar to the pure AFF_{powder} (Fig. S3) but bands at 1385 and 1273 cm^{-1} are probably related to Fe-carboxylate interaction [31,32].

TG analysis of this solid under air atmosphere (Fig. 4) showed a weight loss of 95% with 5% of remaining brown solid Fe_2O_3, suggesting that the solid AFF/Fe_{powder} contains ca. 3.5 wt% of Fe.

On the other hand, TG under N_2 atmosphere showed a gradual decomposition from 150 up to 900 °C leading to a ca. 60% total weight loss (see Fig. S9).

The thermal decomposition of AFF/Fe_{powder} to produce a Fe/carbon composite with application in the steel industry and gas/liquid products with potential use as fuels (Eq. (5)) was investigated.

$$Fe^{3+}_{extracted}/AAF \rightarrow Fe/carbon + Fuels_{(gas/liquid)} \quad (5)$$

Based on previous work [33], thermal decompositions were carried out at 400 °C (where most of organic structures are already decomposed to carbon and volatiles), 600 °C (where carbon structures further deoxygenate and start the reduction of iron oxides) and 800 °C (where carbon reduces oxides to Fe^0 metal).

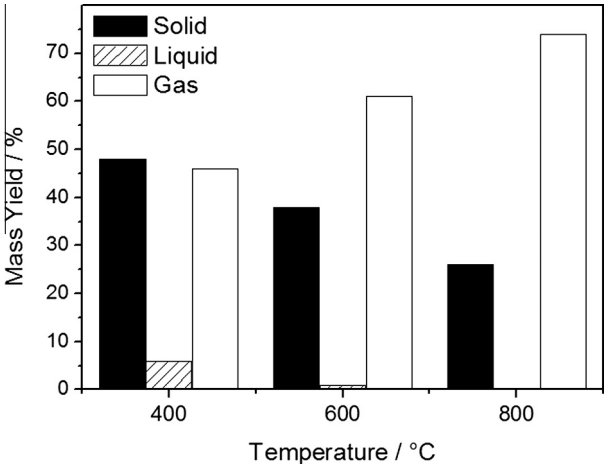

Fig. 5. Product yields (wt%) after thermal treatments of the mixture AAF/Fe_{powder}.

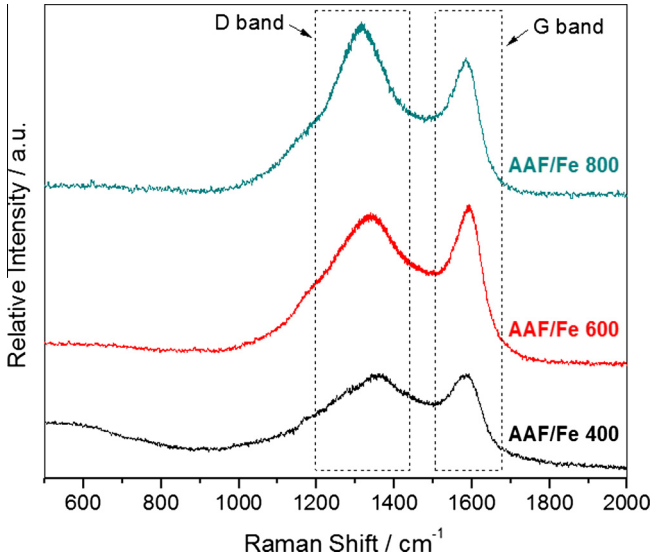

Fig. 6. Raman spectra obtained for the solid products AAF/Fe400, AAF/Fe600 and AAF/Fe800.

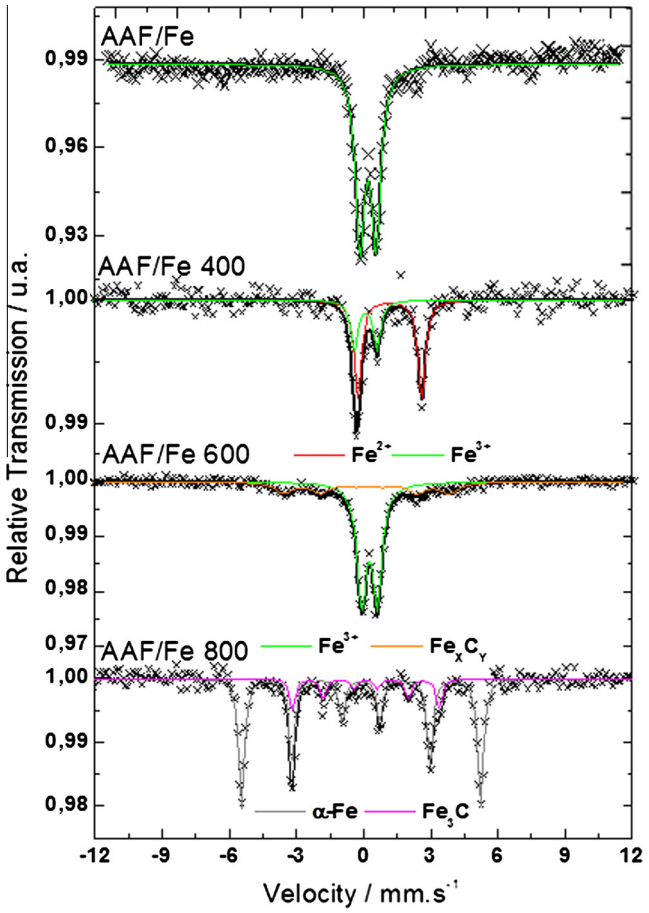

Fig. 7. Mössbauer spectra for solid products.

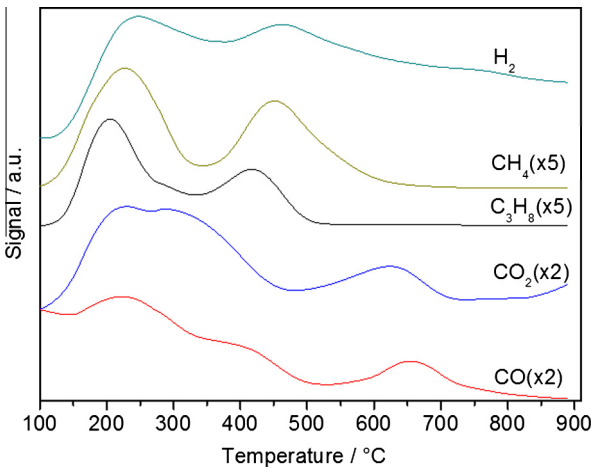

Fig. 8. Gas products identified by TG-MS analysis of the thermal decomposition of AAF/Fe.

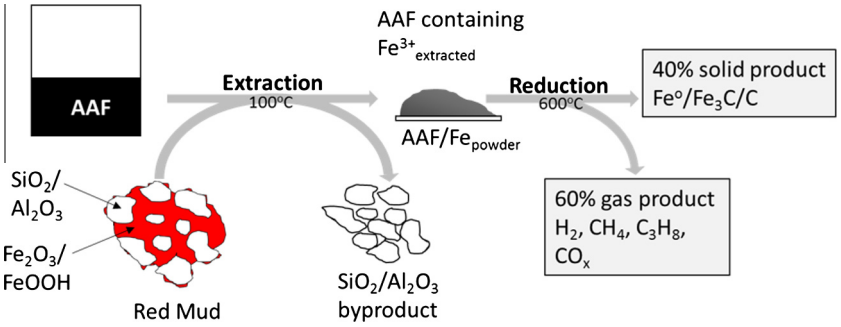

Fig. 9. Reductive extraction combined with the Fe promoted conversion of the organic fraction of AAF.

The product yields (wt%) after thermal treatments of the mixture AAF/Fe_{powder} are shown in Fig. 5.

It can be observed that in all temperatures the main products are solid and gas with small amounts of liquids. As temperature increased to 800 °C, the amount of gas produced increased to 72 wt% whereas the solid decreased to 28% and no significant amount of liquid product was formed.

Raman spectra of solid products obtained at 400, 600 and 800 °C, named AAF/Fe400, AAF/Fe600 and AAF/Fe800 (Fig. 6), showed the two typical bands of carbonaceous materials, *i.e.* G and D bands, related to the formation of more organized graphite like and amorphous carbon, respectively [34]. It can be observed that the intensity of D band of more defective graphene carbon structures increases with temperature. This increase is commonly observed in this temperature range during the decomposition of organics to form carbon materials [35].

Mössbauer spectrum of the precursor system AAF/Fe_{powder} (Fig. 7) showed a typical signal of superparamagnetic highly dispersed Fe^{3+}, which is related to iron species complexed with organic compounds. After thermal treatment at 400 °C, iron was reduced to form 67% of Fe^{2+} and 33% of Fe^{3+} phases dispersed in a black solid. Probably, during thermal treatment, organic matter decomposes to different volatile reducing species, *e.g.* H_2, CO, organics, which can reduce the extracted Fe^{3+} to Fe^{2+} (Eq. (6)).

$$[Fe^{3+}(organics)_n] \rightarrow Fe^{2+}(Fe_3O_4, FeO, Fe^{2+})_{highly\ disp} + CO_x/H_2O/volatiles \quad (6)$$

At 600 °C, iron was further reduced to form metallic Fe as carbide Fe_xC_y (33%) and Fe^{3+} (67%). This high amount of Fe^{3+} is probably formed by oxidation when the obtained solid was exposed to air at room temperature [20]. At 800 °C, Fe^{3+} extracted is completely converted to reduced iron phases Fe^0 and Fe_3C. XRD patterns of these solids confirm the Mössbauer data (Fig. S10).

Besides Fe, solid products likely contains other metals, especially Al (with concentrations lower than 10 wt% related to Fe) and Ti (traces).

TG curves obtained for solid products after thermal treatment (400, 600 and 800 °C) under air atmosphere are shown in Supplementary Material (Fig. S11). The sample AAF/Fe400 showed a gradual weight loss of ca. 25% up to 300 °C, likely due to loss of moisture (adsorbed from air after treatment), followed by a weight loss centered at 380 °C of 50% related to oxidation of carbon. It is interesting to observe that carbon oxidation temperature increased from 380 to 410 and 515 °C for the solids AAF/Fe400, AAF/Fe600 and AAF/Fe800, respectively. These results suggest that carbon formed at 800 °C is more organized and thermally stable. Although carbon content estimation by TG is very limited due to sampling problems and precision, the obtained results suggest carbon content increased to 80% for the solid obtained at 600 °C. On the other hand, carbon content of the solid obtained at 800 °C decreased to 65%, likely due to reaction of carbon with Fe oxides to produce CO_x.

TG-MS analyses of gas products (Fig. 8) showed the presence of different fuel gases, mainly H_2, CH_4, C_3H_8 and also CO/CO_2.

MS signals suggest most of these fuel molecules are produced as two main peaks located in the temperature ranges 150–300 °C and 350–500 °C. These processes are likely related to the decomposition of organics present in AAF to form carbon. At higher temperatures, only the formation of carbon dioxide and monoxide are observed, likely related to the reaction of Fe oxides with carbon to produce Fe metal and carbide, besides CO_x (Eq. (7)).

$$Fe^{3+}/Fe^{2+}oxides + C \rightarrow CO/CO_2 + Fe^0/Fe_3C \quad (7)$$

A calibration of TG-MS was performed with a standard mixture containing these gases (Fig. S12). The obtained results showed the formation of H_2, CH_4, C_3H_8 and CO_x at approximately 58, 10, 9 and 23 mol%, respectively.

The results obtained in this work suggest AAF can be used to extract iron from the waste red mud to produce a solid byproduct containing mainly Al_2O_3 and SiO_2 and a mixture containing $Fe^{3+}_{extracted}$ with organic compounds (Fig. 9).

This mixture with $Fe^{3+}_{extracted}$ can be thermally treated (600 °C) to produce a solid product with 40% yield containing Fe^0/Fe_3C/carbon, which shows a great potential to be used in steel industry as Fe source and especially as fuel due to high carbon content. A gas product with 60% yield is produced, containing mainly H_2 (58 mol%), C_1–C_3 (19 mol%) and CO_x (23 mol%).

4. Conclusions

Aqueous acid waste fraction (AAF) from bio-oil can be used to efficiently extract iron from wastes such as red mud. Thermal treatment of the mixture AAF/Fe at temperatures between 400 and 800 °C, produces a solid composite containing Fe and carbon with potential application in steel industry and also a gas fraction containing H_2, CH_4, C_2H_6 and CO_x with potential use as fuel.

Acknowledgements

Authors thank CAPES, CNPq, SECTES and FAPEMIG for all financial support. To T.A.R. Santos for ^1H NMR analysis.

Appendix A. Supplementary material

Supplementary data associated with this article can be found, in the online version, at http://dx.doi.org/10.1016/j.fuel.2016.06.099.

References

[1] Jayasinghe P, Hawboldt K. A review of bio-oils from waste biomass: focus on fish processing waste. Renew Sustain Energy Rev 2012;16:798–821.
[2] Zhang Q, Chang J, Wang T, Xu Y. Review of biomass pyrolysis oil properties and upgrading research. Energy Convers Manage 2007;48:87–92.

[3] Carpenter D, Westover TL, Czernik S, Jablonski W. Biomass feedstocks for renewable fuel production: a review of the impacts of feedstock and pretreatment on the yield and product distribution of fast pyrolysis bio-oils and vapors. Green Chem 2014;16:384–406.
[4] Venkatakrishnan VK, Degenstein JC, Smeltz AD, Delgass WN, Agrawal R, Ribeiro FH. High-pressure fast-pyrolysis, fast-hydropyrolysis and catalytic hydrodeoxygenation of cellulose: production of liquid fuel from biomass. Green Chem 2014;16:792–802.
[5] Yang SI, Wu MS, Wu CY. Application of biomass fast pyrolysis Part I: Pyrolysis characteristics and products. Energy 2014;66:162–71.
[6] Chen H, Wang G, Chen G. Step collection of bio-oil from pyrolysis of steam exploded sumac marc and activated carbon prepared from pyrolysis residues. Energy Fuels 2003;27:7432–8.
[7] Uzun BB, Sarioglu N. Rapid and catalytic pyrolysis of corn stalks. Fuel Process Technol 2009;90:705–16.
[8] Boucher ME, Chaala A, Roy C. Bio-oils obtained by vacuum pyrolysis of softwood bark as a liquid fuel for gas turbines. Part I: Properties of bio-oil and its blends with methanol and a pyrolytic aqueous phase. Biomass Bioenergy 2000;19:337–50.
[9] Zhang S, Yan Y, Li T, Ren Z. Upgrading of liquid fuel from the pyrolysis of biomass. Bioresour Technol 2005;96:545–50.
[10] Xu R, Ferrante L, Briens C, Berruti F. Bio-oil production by flash pyrolysis of sugarcane residues and post treatments of the aqueous phase. J Anal Appl Pyrol 2011;91:263–72.
[11] Yao C, Dong L, Wang Y, Yu J, Li Q, Xu G, et al. Fluidized bed pyrolysis of distilled spirits lees for adapting to its circulating fluidized bed decoupling combustion. Fuel Process Technol 2011;92:2312–9.
[12] Lian J, Garcia-Perez M, Coates R, Wu H, Chen S. Yeast fermentation of carboxylic acids obtained from pyrolytic aqueous phases for lipid production. Bioresour Technol 2012;118:177–86.
[13] Yao D, Wu C, Yang H, Hu Q, Nahil MA, Chen H, et al. Hydrogen production from catalytic reforming of the aqueous fraction of pyrolysis bio-oil with modified Ni–Al catalysts. Int J Hydrogen Energy 2014;39:14642–52.
[14] Valle B, Remiro A, Aguayo AT, Bilbao J, Gayubo AG. Catalysts of Ni/α-Al_2O_3 and Ni/La_2O_3-αAl_2O_3 for hydrogen production by steam reforming of bio-oil aqueous fraction with pyrolytic lignin retention. Int J Hydrogen Energy 2013;38:1307–18.
[15] Pan C, Chen A, Liu Z, Chen P, Lou H, Zheng X. Aqueous-phase reforming of the low-boiling fraction of rice husk pyrolyzed bio-oil in the presence of platinum catalyst for hydrogen production. Bioresour Technol 2012;125:335–9.
[16] Power G, Gräfe M, Klauber C. Bauxite residue issues: I. Current management, disposal and storage practices. Hydrometallurgy 2011;108:33–45.
[17] Oliveira AAS, Teixeira IF, Ribeiro LP, Tristao JC, Dias A, Lago RM. Magnetic amphiphilic composites based on carbon nanotubes and nanofibers grown on an inorganic matrix: effect on water-oil interfaces. J Braz Chem Soc 2010;21:2184–8.
[18] Oliveira AAS, Tristão JC, Ardisson JD, Dias A, Lago RM. Production of nanostructured magnetic composites based on Fe^0 nuclei coated with carbon nanofibers and nanotubes from red mud waste and ethanol. Appl Catal B 2011;105:163–70.
[19] Teixeira IF, Medeiros TPV, Freitas PE, Rosmaninho MG, Ardisson JD, Lago RM. Carbon deposition and oxidation using the waste red mud: a route to store, transport and use offshore gas lost in petroleum exploration. Fuel 2014;124:7–13.
[20] Costa RCC, Moura FCC, Oliveira PEF, Magalhães F, Ardisson JD, Lago RM. Controlled reduction of red mud waste to produce active systems for environmental applications: heterogeneous Fenton reaction and reduction of Cr(VI). Chemosphere 2010;78:1116–20.
[21] Karimi E, Teixeira IF, Gomez A, de Resende E, Gissane C, Leitch J, et al. Synergistic co-processing of an acidic hardwood derived pyrolysis bio-oil with alkaline Red Mud bauxite mining waste as a sacrificial upgrading catalyst. Appl Catal B Environ 2014;145:187–96.
[22] Karimi E, Teixeira IF, Ribeiro LP, Gomez A, Lago RM, Penner G, et al. Ketonization and deoxygenation of alkanoic acids and conversion of levulinic acid to hydrocarbons using a Red Mud bauxite mining waste as the catalyst. Catal Today 2012;190:73–88.
[23] Kumar S, Kumar R, Bandopadhyay A. Innovative methodologies for the utilisation of wastes from metallurgical and allied industries. Resour Conserv Recycl 2006;48:301–14.
[24] Liu W, Yang J, Xiao B. Application of Bayer red mud for iron recovery and building material production from alumosilicate residues. J Hazard Mater 2009;161:474–8.
[25] Krimpalis S, Papadopoulos N, Efthimiadis KG, Karagianni CS, Hristoforou E. Magnetic properties in red mud after thermal treatment. J Optoelectron Adv Mater 2008;10:1085–8.
[26] Wang S, Ang HM, Tadé MO. Novel applications of red mud as coagulant, adsorbent and catalyst for environmentally benign processes. Chemosphere 2008;72:1621–35.
[27] Liu W-J, Tian K, Jiang H, Zhang X-S, Ding H-S, Yu H-Q. Selectively improving the bio-oil quality by catalytic fast pyrolysis of heavy-metal-polluted biomass: take copper (Cu) as an example. Environ Sci Technol 2012;46:7849–56.
[28] Bordoloi N, Narzari R, Chutia RS, Bhaskar T, Kataki R. Pyrolysis of *Mesua ferrea* and *Pongamia glabra* seed cover: characterization of bio-oil and its sub-fractions. Bioresour Technol 2015;178:83–9.
[29] Özbay G, Pekgözlü A, Ozcifci A. The effect of heat treatment on bio-oil properties obtained from pyrolysis of wood sawdust. Eur J Wood Wood Prod 2015;73:507–14.
[30] Elkasabi Y, Mullen CA, Jackson MA, Boateng AA. Characterization of fast-pyrolysis bio-oil distillation residues and their potential applications. J Anal Appl Pyrol 2015;114:179–86.
[31] Deacon JB, Phillips RJ. Relationships between the carbon-oxygen stretching frequencies of carboxylato complexes and the type of carboxylate coordination. Coord Chem Rev 1980;33:227–50.
[32] Sutton CCR, da Silva G, Franks GV. Modeling the IR spectra of aqueous metal carboxylate complexes: correlation between bonding geometry and stretching mode wavenumber shifts. Chem Eur J 2015;21:6801–5.
[33] Teixeira APC, Tristao JC, Araujo MH, Oliveira LCA, Moura FCC, Ardisson JD, et al. Iron: a versatile element to produce materials for environmental applications. J Braz Chem Soc 2012;23:1579–93.
[34] Pimenta MA, Dresselhaus G, Dresselhaus MS, Cancado LG, Jorio A, Saito R. Studying disorder in graphite-based systems by Raman spectroscopy. Phys Chem Chem Phys 2007;9:1276–90.
[35] Li X, Hayashi J-I, Li C-Z. FT-Raman spectroscopic study of the evolution of char structure during the pyrolysis of a Victorian brown coal. Fuel 2006;85:1700–7.